Aerodynamic Optimization of Mach 0.8 Transonic Truss-Braced Wing Aircraft using Variable Camber Continuous Trailing Edge Flap

Juntao Xiong*
KBR Wyle, Inc., Moffett Field, CA 94035
Nhan Nguyen†
NASA Ames Research Center, Moffett Field, CA 94035
Robert E. Bartels‡
NASA Langley Research Center, Hampton, VA 23681

This paper presents an aerodynamic optimization study of the Mach 0.8 Transonic Truss-Braced Wing (TTBW) aircraft with Variable Camber Continuous Trailing Edge Flap (VCCTEF). The VCCTEF is a novel wing shaping control concept to improve aircraft aerodynamic efficiency. Drag reduction studies are conducted for two different VCCTEF configurations with 6- and 10-spanwise sections, respectively. A simple VCCTEF actuator weight model is used to account the weight penalty of the actuator in the design for the Mach 0.8 TTBW aircraft. A vortex-lattice model of the Mach 0.8 TTBW aircraft is developed with transonic small disturbance, integral boundary-layer, and wing-strut interference corrections for rapid aerodynamic performance evaluations. The VSPAERO model has been validated against the wind tunnel test data. The optimization results show that the 6-spanwise sections VCCTEF provides a relatively better solution for drag reduction when the actuator weight penalty is considered. A high-fidelity CFD solver FUN3D is used to verify the VCCTEF optimization design.

I. Introduction

Research and development of high aspect ratio wing transport designs has placed a greater emphasis on the studies of aeroelasticity and flutter owing to the increase in the wing flexibility as the wing aspect ratio increases. These studies have sought to develop methods and tools for aeroelasticity by laying the foundation for more modern high aspect ratio wing aircraft such as the Transonic Truss-Braced Wing (TTBW).[1,2,3] The Boeing developed Mach 0.8 TTBW aircraft[4] shown in Figure 1 is designed to be aerodynamically efficient by employing an aspect ratio of about 19.55, which is significantly greater than those of conventional aircraft cantilever wings. The main idea is to use truss structures to alleviate the wing root bending moment, so that a significant increase in the wing aspect ratio could be afforded. The design of a truss-braced wing is a Multidisciplinary Design Analysis and Optimization (MDAO) process that strives to achieve a delicate balance between aerodynamic and structural efficiencies. The MDAO studies have been conducted at each stage to improve the wing aerodynamics, structural efficiency, and flight performance. These MDAO studies have refined the geometry of the wing and configuration layout and have involved trade studies involving minimizing induced drag, profile drag, and wave drag due to the addition of the main strut and jury struts. One option for managing the aeroelastic behavior of the aircraft is through control system design. The control system could be made to both suppress undesirable motion and shape the flexible structure in pursuit of improved performance goals.

*Aerospace Engineer, Intelligent System Division, juntao.xiong@nasa.gov, AIAA Member
†Senior Research Scientist and Technical Group Lead, Intelligent Systems Division, nhan.t.nguyen@nasa.gov, Associate Fellow AIAA
‡Research Aerospace Engineer, NASA Langley Research Center, MS 340, robert.e.bartels@nasa.gov, AIAA Senior Member

Figure 1 Boeing SUGAR Mach 0.8 Transonic Truss-Braced Wing (TTBW) Aircraft Concept

The use of variable camber continuous trailing edge flap (VCCTEF) proposed by Nguyen in 2010[5,6] for active control of aeroelastic wings such as suppressing flutter, stabilizing the vehicle response to gusts, and reducing drag have been studied.[7,8,9,10] Nguyen et al.[7] first demonstrated the Common Research Model (CRM) real-time drag optimization wind tunnel experiment using the VCCTEF at low speed. Lebofsky et al.[8] used the VCCTEF with optimized deflections for load alleviation for the TTBW aircraft. Ting et al.[9] conducted drag optimization study using generic transport model (GTM) with VCCTEF. An 8.4% drag reduction can be achieved using a parabolic flap deflection profile configuration with three-cambered-segments, but this study does not account for the actuator weight penalty. Bartels et al.[10] utilized the VCCTEF with feedback control system to enhance the aeroelastic stability and performance of the TTBW aircraft. A previous aerodynamic optimization study[11] was conducted for the Mach 0.745 TTBW aircraft with the VCCTEF. Those studies indicate the VCCTEF system offers potential payoff in drag reduction by actively controlling the shape of the wing for the TTBW aircraft.

In this paper we perform an aerodynamic optimization study of Mach 0.8 TTBW aircraft with the VCCTEF. Drag reduction studies are conducted for two different VCCTEF configurations with 6- and 10-spanwise sections, respectively. A simple VCCTEF actuator weight model based on aircraft data is used to estimate the weight penalty of the actuator in the design for the Mach 0.8 TTBW aircraft. A vortex-lattice model of the Mach 0.8 TTBW aircraft is developed with transonic small disturbance, integral boundary-layer, and wing-strut interference corrections for rapid aerodynamic performance evaluations. A high-fidelity CFD solver FUN3D is used to verify the VCCTEF optimization design.

II. Aerodynamic Model of the Truss-Braced Wing

A. VSPAERO Model

In order to develop a rapid aeroelastic analysis that facilitates a vehicle MDAO process, a lower-fidelity aerodynamic model of the TTBW is necessary. VSPAERO[12] is a solver that includes both the vortex lattice method and the full panel method based on generalized vortex rings. The core VSPAERO solver is based on an agglomerated multi-pole approach, coupled with a preconditioned linear solver, to reduce solution times. Adaptive wakes, time-accurate, unsteady analyses, and propeller modeling are all supported. VSPAERO is part of the OpenVSP design package and is freely available under the NASA open source license. Figure 2 illustrates the Mach 0.8 TTBW VSPAERO models. Figure 3 shows the differential pressure coefficient contour at Mach 0.8 and an angle of attack of 2° for the VSPAERO vortex-lattice model.

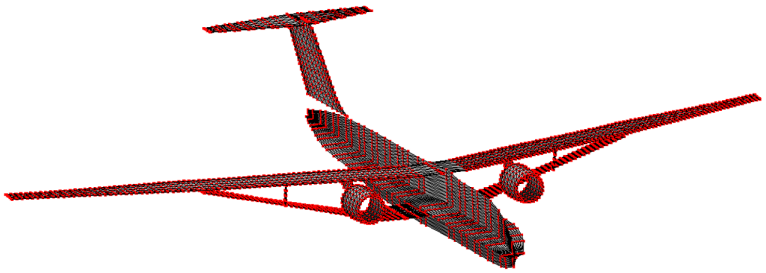

Figure 2 VSPAERO Model of Mach 0.8 TTBW

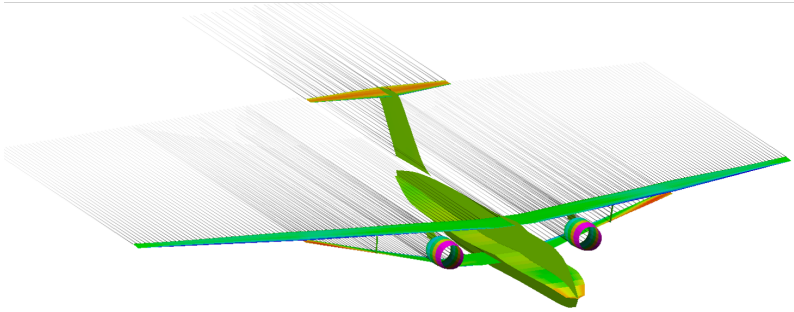

Figure 3 Differential Pressure Coefficient Contour of VSPAERO Model of Mach 0.8 TTBW

B. Transonic and Viscous Flow Correction

Because of the missing transonic effect in the linear potential flow method, a method for transonic and viscous corrections has recently been developed.[13,14,15] In this method, a full-configuration aerodynamic model can be based on the vortex-lattice or panel method. The wing is discretized into several spanwise sections at which the section lift coefficients computed by the potential flow method are used to correct for the transonic and viscous flow effects.[14,15] The transonic and viscous correction method is an iterative process to compute the incremental section lift coefficient due to transonic and viscous flow by a virtual re-twist of the individual wing sections to account for the accompanied change in the effective local angle of attack.[15] Implementation of the correction begins by initializing the virtual twist angle due to transonic and viscous corrections, $\gamma(y)$, to zero. The effective 2D angle of attack is then calculated for each airfoil using,

$$\alpha_{2D}(y) = \alpha_0(y) + \frac{c_{l_{3D}}(y)}{c_{l_\alpha}} - \gamma(y), \tag{1}$$

where α_{2D} is the effective airfoil angle of attack, α_0 is the the airfoil zero-lift angle of attack, $c_{l_{3D}}$ is the section lift coefficient obtained via VSPAERO, and c_{l_α} is the 2D lift curve slope corrected for sweep as follows:

$$c_{l_\alpha} = \frac{2\pi}{\sqrt{1 - M_\Lambda^2}}. \tag{2}$$

Here, M_Λ is the Mach number based on the mid-chord sweep angle. Each airfoil is analyzed by the TSD/IBL model at the effective angle of attack. The transonic flow correction is handled by the transonic small disturbance (TSD) code TSFOIL.[16] This code is loosely coupled to the in-house integral boundary layer (IBL) code developed by Nguyen et al.[13] to correct for the viscous flow interaction with the transonic shock on an airfoil. Optionally, the correction method can be performed using the 2D Euler CFD code MSES with an integral boundary layer method developed by Mark Drela[17] as an available option.. The virtual twist angle is then updated for each section according to:

$$\gamma_{i+1}(y) = \gamma_i(y) + \frac{c_{l_{2D_i}}(y) - c_{l_{3D_i}}(y)}{c_{l_\alpha}}, \tag{3}$$

where $c_{l_{2D_i}}$ corresponds to the airfoil lift coefficient calculated by TSFOIL or MSES for iteration i.

The coupling and iterative update process is repeated until the 3D wing section lift and the 2D airfoil lift computed by the TSD/IBL correction method converge for all sections. Wave and friction drag are calculated by the TSD/IBL correction method, whereas lift, pitching moment, and induced drag are calculated by the VSPAERO model. The flow chart of the transonic and viscous flow correction method is shown in Figure 4.[15] An extensive validation of the transonic and viscous flow correction method has been performed to compare the method against RANS CFD solvers.[18] The solution method agrees quite well in terms of key aerodynamic parameters and pressure distribution results. The major advantage of using a potential flow method coupled to the transonic and viscous flow corrections is the computational efficiency of the method, which is several orders of magnitude faster than a typical RANS CFD solution. This computational efficiency becomes highly important when the potential flow solver is coupled to a structural finite-element model for aero-structural modeling analysis.

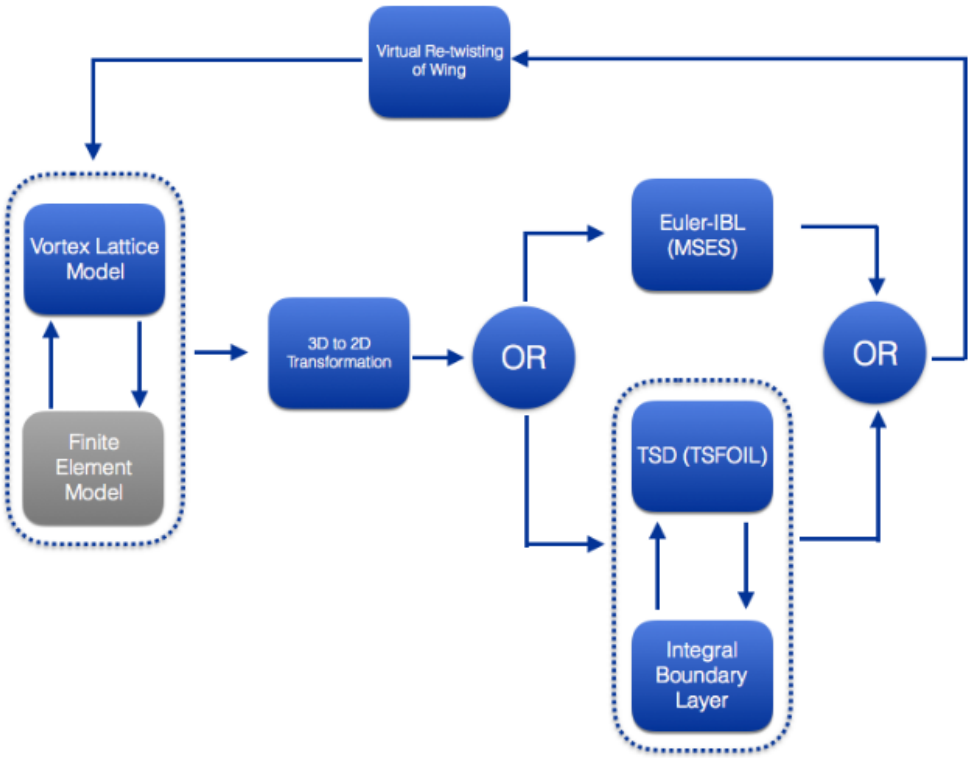

Figure 4 Transonic and Viscous Correction Flow Chart

C. Wing-Strut Interference Aerodynamic Correction

The transonic and viscous flow corrections using the TSD/IBL method are generally valid for a single-element airfoil. The TTBW configuration is a complex geometry that includes a strut juncture region where the effect of interference aerodynamics can influence the overall aerodynamic performance of the aircraft. As the strut approaches the wing from below, the transonic and viscous flow corrections using the TSD/IBL method are no longer valid due to the interactions between the wing airfoil and strut airfoil.[18,19] To account for these interference aerodynamics, CFD models of the wing-strut configuration and the wing-alone configuration of the TTBW aircraft are developed using FUN3D. To isolate the interference aerodynamic effect for the wing and strut, the nacelle, the pylon, and the horizontal tail are removed from the models. Surface pressure coefficients are computed for both configurations at various wing stations. By comparing the wing-strut data to the wing-alone data, it is seen that the presence of the strut induces a suction peak along the lower surface of the wing near the wing-strut juncture.[19]

A wing-strut interference correction model for Mach 0.8 TTBW is developed to correct the VSPAERO model.[20] The correction method is applied to the VSPAERO+TSD/IBL model to update the section lift, drag, and pitching moment coefficient of each wing section.

The interference correction, Δc_{IC}, that is applied to the model is calculated using the following equation,

$$\Delta c_{IC} = \Delta c_{FUN3D} - \Delta c_{VSPAERO+TSD/IBL}, \tag{4}$$

where c represents a key aerodynamic parameter such as c_l, c_d, and c_m and Δ represents the change in the given parameter between the wing-strut configuration and wing-alone configuration.

D. Aerodynamic Analysis of Cruise Shape Geometry

The VSPAERO model is used for the aerodynamic analysis of the cruise 1g shape TTBW geometry for the Mach 0.8 TTBW aircraft configuration.. Wind tunnel test data of the cruise shape geometry in NASA Ames 11-Ft Transonic Wind Tunnel are available for validation of the VSPAERO models. Figure 5 shows the plots of the lift and drag coefficients computed by VSPAERO for Mach 0.8 and a Reynolds number of 2.17 million with and without all the corrections. The differences between the simulation results of VSPAERO+TSD/IBL model with and without interference corrections are small. The computed results are compared to Run 378 wind tunnel data. The lift coefficient is somewhat overpredicted. With all the corrections applied to the VSPAERO model for transonic viscous flow and wing-strut interference aerodynamics, the lift and drag coefficients match well to the wind tunnel data, although there is a small discrepancy in the drag polar at lower lift coefficients. The VSPAERO+TSD/IBL with the wing-strut interference correction model can be used as a fast and reliable tool for the TTBW aircraft conceptual analysis and design.

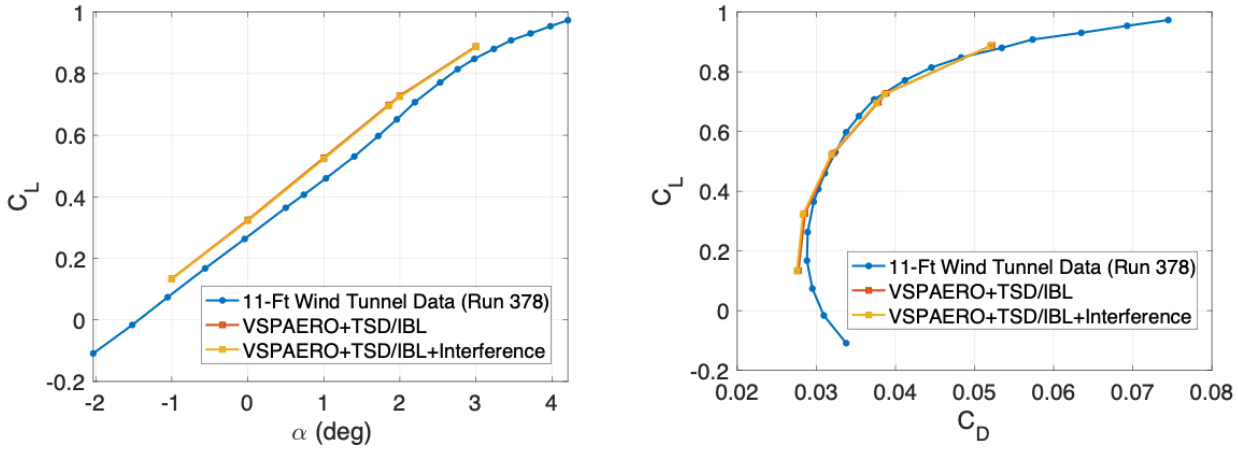

(a) Lift Curve

(b) Drag Polar

Figure 5 Mach 0.8 TTBW Lift Curve and Drag Polar at Mach 0.8 and $Re = 2.17 \times 10^6$

III. Drag Optimization Study

A. Drag Optimization

The goal of the optimization scheme is to minimize the drag coefficient of the 1g shape geometry for the Mach 0.8 TTBW aircraft at three different flight conditions via changing VCCTEF deflection angles. Lift constraints are added to the optimization algorithm, such that $\left|C_{L_j} - C_{L_{d_j}}\right| < 0.001$, where $C_{L_{d_j}}$ is the design lift coefficient, j is the design point index. In this study, three different flight conditions corresponding to Mach 0.8 at 40,000 ft with 20%, 50%, and 80% fuel are selected for the drag optimization. The lift coefficients at the three flight conditions are $C_{L_1} = 0.661$, $C_{L_2} = 0.695$, and $C_{L_3} = 0.729$. A gradient-based optimization scheme utilizing the steepest descent method is used with the cost function as described below:

$$J(\alpha, \delta_i) = C_D, \tag{5}$$

where C_D is the aircraft drag coefficient from the VSPAERO model of the 1g shape geometry, δ_i represents the VCCTEF deflection angles along the spanwise direction. In this paper the VCCTEF deflection angles are directly used as design variables. The steepest descent algorithm for updating the design variables can be represented by the following equations:

$$\alpha_{k+1} = \alpha_k - \epsilon \frac{\partial J}{\partial \alpha} \tag{6}$$

$$\delta_{i_{k+1}} = \delta_{i_k} - \epsilon \frac{\partial J}{\partial \delta_i} \tag{7}$$

Here, the design variable at iteration k is updated based on the partial derivative of the cost function with respect to the design variable, which is calculated using a small-perturbation, second-order central difference scheme, and ϵ is a step size term.

Figure 6 shows a NASA supercritical SC(2) transonic airfoil illustrated with a 2-cambered segment VCCTEF as the exact TTBW airfoil cannot be shown. The deflection angle is positive when the flap is deflected downward. In this paper, the drag reduction studies are conducted for two different VCCTEF configurations with 6- and 10-spanwise sections, respectively. In addition, a plain flap configuration with 6 spanwise sections is also considered. The planforms of the three configuration are shown in Fig. 7.

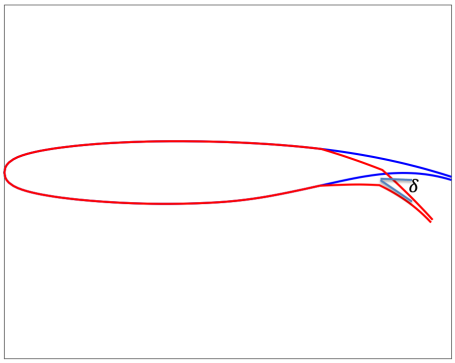

Figure 6 2-cambered segment VCCTEF

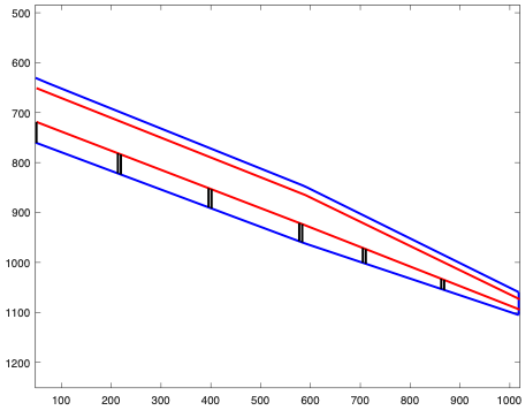

(a) 6-Spanwise Plain Flap Layout

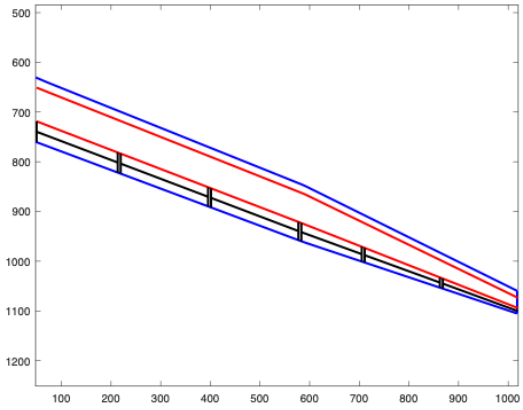

(b) 6-Spanwise Two-Segment Flap Layout

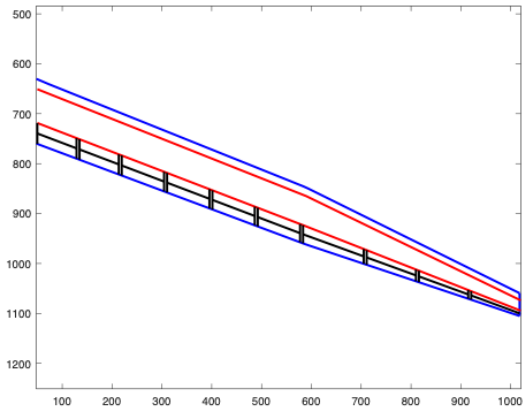

(c) 10-Spanwise Two-Segment Flap Layout

Figure 7 VCCTEF Configurations

B. VCCTEF Actuator Weight Model

In order to trade the drag reduction benefit of the VCCTEF against the weight increase in the actuator system, a representative actuator weight model is developed. The weight of a control surface is due to both the structural weight of the control surface and the weight of the servo-actuator system. Available structural weight data for a transport is used to scale the control surface weight model for the VCCTEF. An average weight per unit surface area of 5.2630 psf is estimated from this data source. This weight data is based on an aluminum structure. For composite structures, an average weight reduction of 28% is used. Therefore, the average weight per unit surface area for composite structures is estimated to be 3.7893 psf.

For the Mach 0.8 TTBW, the total surface area of the six-spanwise two-segment VCCTEF as shown in Figure is computed to be 220.2 ft^2. This results in a control surface weight of about 835 lbs. A clean wing without control surfaces that occupies the same surface area is assumed to be half of the control surface weight. Therefore, a weight penalty due to the control surface weight is 416 lbs.

To estimate the servo-actuator weight, a hinge moment analysis is conducted. The hinge moments for the flap elements are only computed for drag optimization. Based on the flap deflections obtained from the drag optimization for the 6-VCCTEF layout, the hinge moments computed by the Theodorsen's theory[21] are presented in 1.

Table 1 Hinge Moments of Flap Elements of 6-VCCTEF Layout

	Spanwise Flap Section					
	1	2	3	4	5	6
Inner Flap Hinge Coefficient	−0.1147	−0.1146	−0.01055	−0.1132	−0.1406	−0.1401
Outer Flap Hinge Coefficient	−0.0353	−0.0381	−0.0381	−0.0263	−0.0327	−0.0326
Inner Flap Deflection	−0.365°	−0.265°	−0.275°	−0.435°	−0.8°	−1.415°
Outer Flap Deflection	−0.73°	−0.53°	−0.55°	−0.87°	−1.6°	−2.83°
Inner Flap Hinge Moment (ft-lbs)	151	110	105	92	131	112
Outer Flap Hinge Moment (ft-lbs)	15	11	12	13	30	52

Servo-actuator drives for transport aircraft can be classified as hydraulic actuator, electro-mechanical actuator, or shape memory actuator (SMA). SMA has a significant torque-to-weight ratio advantage, but has a much slower bandwidth that is not suitable for flight control requirements.[22] As an example, SMA with 500 ft-lbs could weigh about 8 lbs. On the other hand, an EMA with gear box for a 160 ft-lbs rated torque could weigh 41 lbs. The motor rated torques are sized based on the hinge moments from Table 1. Thus, a motor with a rated torque that exceeds 15 ft-lb torque should be sufficient.

Assuming that the two outboard spanwise flap sections are multi-functional capable for both drag optimization and roll control, there is no weight penalty due to these two outboard spanwise flap sections. Thus, the total servo weight for SMA is 80 lbs and the total weight for EMA is 410 lbs. The total weight of the flap system is the sum of the structural weight and the servo-actuator weight. The weight model is described by

$$W_{flap} = f_{unc} W_{structue} + n_{flap} W_{servo} \tag{8}$$

where f_{unc} is a factor to account for weight uncertainty which is assumed to be 1.5, $W_{structure}$ is the weight penalty of the control surfaces (control surface weight minus the wing weight occupying the same area) which is estimated to be 416 lbs, n_{flap} is the number of flaps for drag optimization minus the number of flaps used for both drag optimization and roll control, and W_{servo} is the weight of a servo-actuator which is assumed to be 8.1 lbs for SMA and 41 lbs for EMA. Table 2 shows the total weight and updated flight condition for the three VCCTEF layouts. For the purpose of weight-drag trade used in the drag optimization, the EMA weight estimates are used.

Table 2 Actuator weight and Flight Conditions

	$n_{spanwisesection}$	$n_{flaptotal}$	n_{flap}	W_{EMA}	$W_{EMA}/W_{w/a}$	q (psf)	h (ft)	$Re(\times 10^6)$
1g	-	-	-	-	-	175.5	40,000	14.0
6-VCCTEF-Plain	6	6	4	829	0.0092	177.1	39,810	14.1
6-VCCTEF	6	12	10	1034	0.0115	177.5	39,770	14.1
10-VCCTEF	10	20	18	1363	0.0151	178.2	39,680	14.2

C. Optimization Results

The aerodynamic parameters are presented in the Table 3 - 5. Table 6 - 8 show the VCCTEF deflection angles for every design cases. The deflection angles for the inner and outer segments are both listed for the 6-VCCTEF-12DV case. The deflection angle of the outer cambered segment is twice as the inner cambered segment for the circular VCCTEF. The deflection angle of the outer cambered segment is three time as the inner cambered segment for the parabolic VCCTEF. In these tables *DV* means the deflection angles are directly used as design variables. The optimization results show that the 10-spanwise sections VCCTEF has largest absolute drag coefficient reduction, however, the 6-spanwise sections VCCTEF, especially when the deflection angles of the inner and outer segments are directly used as design variables, provides a relatively better solution for the drag reduction when the actuator weight penalty is considered.

Overall, the drag reductions for 6-VCCTEF-12DV are 1.90%, 1.66%, and 2.14% at the three flight conditions. It should be noted that the plain flap configuration is the simplest among the flap configurations studied. It offers a drag reduction of 1.48%, 1.26%, and 1.66% at the three flight conditions.

Table 3 VCCTEF Optimization Results from VSPAERO for $C_{L_1} = 0.661$

	C_L	C_D	α (deg)	VSPAERO C_D Reduction (counts)	$\Delta C_D/C_{D_{1g}}$	D (lbs)	$\Delta D/D_{1g}$	L/D
1g	0.661	0.03160	1.495	-	-	4095.878	-	20.918
6-VCCTEF-Plain-6DV	0.661	0.03082	2.1583	7.5	2.37%	4035.121	1.48%	21.426
6-VCCTEF-Circular	0.661	0.03076	2.2339	8.4	2.66%	4032.436	1.55%	21.489
6-VCCTEF-Parabolic	0.661	0.03074	2.235	8.6	2.72%	4029.815	1.61%	21.503
6-VCCTEF-12DV	0.661	0.03065	2.1607	9.5	3.01%	4018.016	1.90%	21.566
10-VCCTEF-20DV	0.661	0.03059	2.201	10.1	3.20%	34026.000	1.71%	21.6084

Table 4 VCCTEF Optimization Results from VSPAERO for $C_{L_2} = 0.695$

	C_L	C_D	α (deg)	VSPAERO C_D Reduction (counts)	$\Delta C_D/C_{D_{1g}}$	D (lbs)	$\Delta D/D_{1g}$	L/D
1g	0.695	0.03250	1.79	-	-	4212.533	-	21.385
6-VCCTEF-Plain-6DV	0.695	0.03179	2.407	7.1	2.15%	4159.379	1.26%	21.855
6-VCCTEF-Circular	0.695	0.03175	2.512	7.5	2.31%	4159.379	1.42%	21.890
6-VCCTEF-Parabolic	0.695	0.03173	2.496	7.7	2.37%	4152.839	1.48%	21.903
6-VCCTEF-12DV	0.695	0.03160	2.279	9.0	2.80%	4150.223	1.66%	21.994
10-VCCTEF-20DV	0.695	0.03153	2.305	9.7	2.98%	4169.679	1.49%	22.042

Table 5 VCCTEF Optimization Results from VSPAERO for $C_{L_3} = 0.729$

	C_L	C_D	α (deg)	VSPAERO C_D Reduction (counts)	$\Delta C_D/C_{D_{1g}}$	D (lbs)	$\Delta D/D_{1g}$	L/D
1g	0.729	0.03450	2.025	-	-	4471.766	-	21.130
6-VCCTEF-Plain-6DV	0.729	0.03362	2.655	8.8	2.55%	4397.43	1.66%	21.685
6-VCCTEF-Circular	0.729	0.03352	2.735	9.8	2.84%	4390.322	1.73%	21.748
6-VCCTEF-Parabolic	0.729	0.03349	2.663	10.1	2.93%	4394.255	1.82%	21.768
6-VCCTEF-12DV	0.729	0.03338	2.540	11.2	3.25%	4375.901	2.14%	21.839
10-VCCTEF-20DV	0.729	0.03339	2.5671	12.0	3.48%	4382.630	1.99%	21.892

Table 6 VCCTEF Deflection Angles (deg.) for $C_{L_1} = 0.661$

	Flap 1	Flap 2	Flap 3	Flap 4	Flap 5	Flap 6				
6-VCCTEF-Plain-6DV	-1.3	-1.7	-2.2	-2.3	-2.1	-0.9				
6-VCCTEF-Circular	-2.0	-2.4	-2.6	-2.3	-1.6	-0.3				
6-VCCTEF-Parabolic	-1.5	-1.9	-2.3	-2.0	-1.8	-0.7				
6-VCCTEF-12DV	-0.1/-2.1	-0.9/-2.2	-2.1/-2.3	-1.5/-2.0	-1.2/-1.3	-0.6/-1.0				
	Flap 1	Flap 2	Flap 3	Flap 4	Flap 5	Flap 6	Flap 7	Flap 8	Flap 9	Flap 10
10-VCCTEF-Chebyshev	-1.3	-1.6	-1.9	-2.1	-2.2	-2.1	-2.0	-1.6	-1.1	-0.4

Table 7 VCCTEF Deflection Angles (deg.) for $C_{L_2} = 0.695$

	Flap 1	Flap 2	Flap 3	Flap 4	Flap 5	Flap 6				
6-VCCTEF-Plain-6DV	-0.1	-1.8	-1.9	-2.0	-2.1	-2.2				
6-VCCTEF-Circular	-0.8	-0.6	-0.6	-0.9	-1.7	-3.0				
6-VCCTEF-Parabolic	-1.0	-1.0	-1.1	-1.2	-1.3	-1.5				
6-VCCTEF-12DV	-0.2/-1.6	-1.2/-1.3	-1.5/-1.5	-1.4/-1.5	-1.6/-2.4	-1.6/-2.0				
	Flap 1	Flap 2	Flap 3	Flap 4	Flap 5	Flap 6	Flap 7	Flap 8	Flap 9	Flap 10
10-VCCTEF-Chebyshev	-1.0	-0.8	-0.6	-0.5	-0.5	-0.7	-1.1	-1.7	-2.4	-3.5

Table 8 VCCTEF Deflection Angles (deg.) for $C_{L_3} = 0.729$

	Flap 1	Flap 2	Flap 3	Flap 4	Flap 5	Flap 6				
6-VCCTEF-Plain-6DV	-0.2	-1.0	-1.1	-1.2	-1.2	-1.3				
6-VCCTEF-Circular	-0.0	0.2	0.2	-0.1	-1.0	-2.3				
6-VCCTEF-Parabolic	-0.5	-0.7	-0.6	-0.8	-1.5	-2.5				
6-VCCTEF-12DV	-0.1/-0.6	-1.1/-1.5	-1.2/-1.3	-0.9/-1.3	-1.1/-1.8	-1.8/-2.2				
	Flap 1	Flap 2	Flap 3	Flap 4	Flap 5	Flap 6	Flap 7	Flap 8	Flap 9	Flap 10
10-VCCTEF-Chebyshev	-0.3	-0.1	0.1	0.2	0.2	0.0	-0.2	-0.7	-1.3	-2.1

D. High-fidelity CFD Validation

To ensure the optimized VCCTEF deflection angles are valid, a validation study using high-fidelity CFD solver FUN3D is performed. The computational fluid dynamics code used in this study is FUN3D,[23,24] which solves the unsteady three-dimensional Navier-Stokes equations on mixed-element grids using a vertices-centered finite-volume method. Information exchange for flow computation on different partitions using multiple CPUs is implemented through the MPI (Message Passing Interface) protocol. It employs an implicit upwind algorithm in which the inviscid fluxes are obtained with a flux-difference-splitting scheme. At interfaces delimiting neighboring control volumes, the inviscid fluxes are computed using an approximate Riemann solver based on the values on either side of the interface. The Roe flux difference splitting[25] is used in the current study. For second-order accuracy, interface values are obtained by extrapolation of the control volume centroidal values, based on gradients computed at the mesh vertices, using an unweighted least squares technique. The Venkatakrishnan[26] limiter is used in the current study to limit the reconstructed values when necessary. In this study the tetrahedral mesh with prism layers are used. In FUN3D, for tetrahedral meshes, the full viscous fluxes are discretized using a finite-volume formulation in which the required velocity gradients on the dual faces are computed using the Green-Gauss theorem. The solution at each time-step is updated with a backwards Euler time-differencing scheme. At each time step, the system of equations is approximately solved with either a multi-color point-implicit procedure or an implicit-line relaxation scheme. Local time-step scaling is employed to accelerate convergence to steady-state. To model turbulent flows, the one-equation model of Spalart-Allmaras[27] (S-A) is used in this study.

Deflected control surfaces are created using the process developed in Ref.[10] The various control surfaces undergo rigid body rotations about the hinge line. A radial basis function smoother applied between flap segments ensures surface continuity between flaps. The surface with the commanded flap rotations is input into the FUN3D code and the volume mesh is deformed. Figure 8 illustrates the planform of the 6-spanwise VCCTEF configuration of the CFD mesh.. Figure 9 shows the close view of the CFD mesh for one of the deformed geometries.

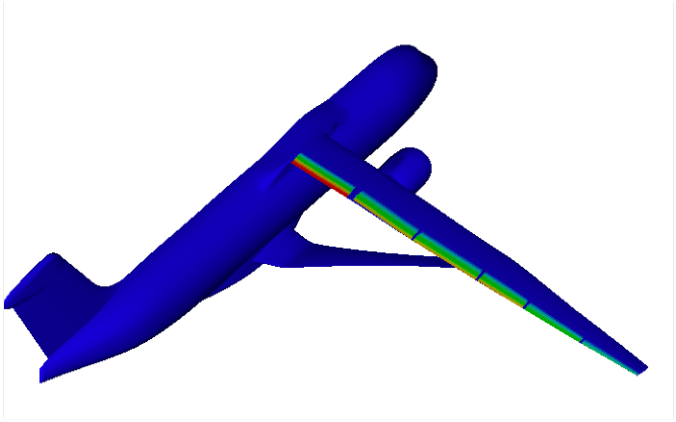

Figure 8 VCCTEF Deflection Layout

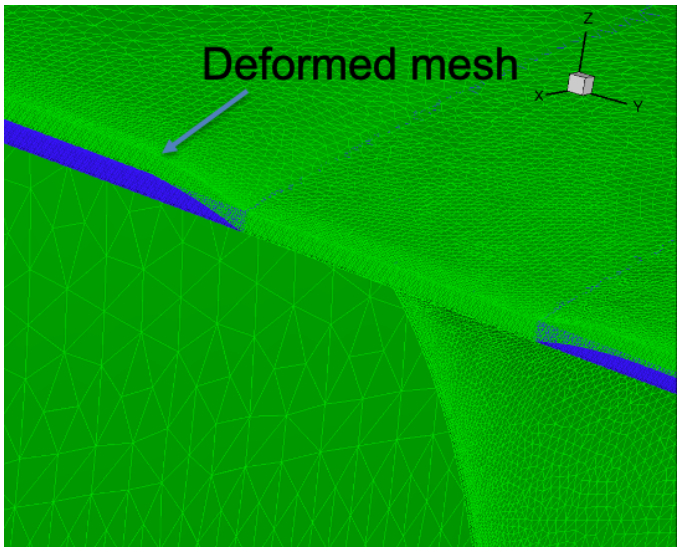

Figure 9 Close View of Deformed CFD Mesh

Figures 10-12 present the pressure contour comparison of the Jig and 6-VCCTEF-12DV design cases at the three design points $C_{L_1} = 0.68$, $C_{L_2} = 0.73$ and $C_{L_3} = 0.78$. The optimized VCCTEF deflections result in a more uniform distribution of the pressure on the aircraft wing surface and thereby helps reduce the drag of the aircraft at the three design conditions.

Table 9- 11 lists the FUN3D simulation results at the three flight design conditions. The optimized VCCTEF deflection results in a drag coefficient reduction of 8.6 counts, 7.6 counts, and 10.1 counts at the three flight conditions as compared to the baseline 1g geometry. The drag reduction results computed by FUN3D agree well with the VSPAERO results. The difference in the drag coefficient ranges from 0.9 to 1.4 counts between the VSPAERO and FUN3D simulations. This confirms the optimization results found by the VSPAERO model.

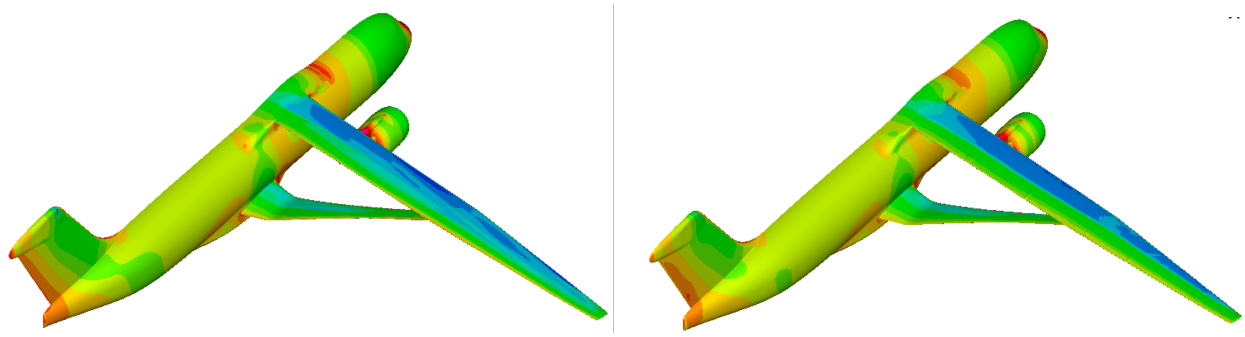

(a) 1g (b) 6-VCCTEF-12DV

Figure 10 Pressure Coefficient Contour on the TTBW Geometries at Mach 0.8 and $C_{L_1} = 0.661$

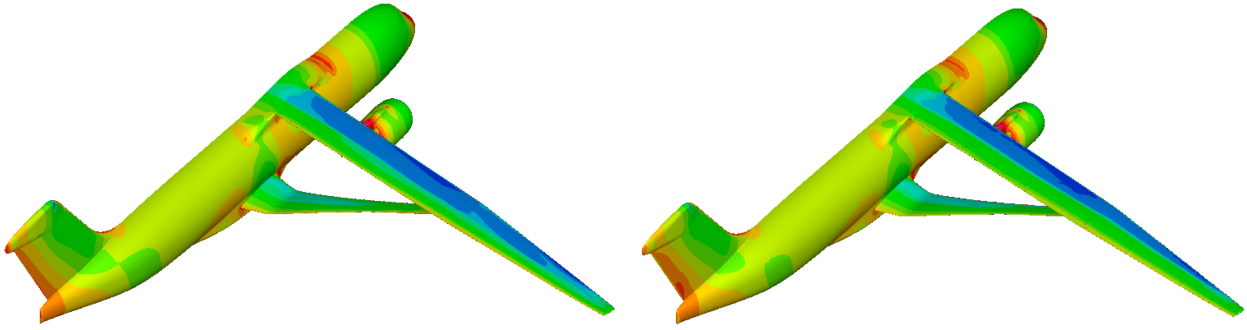

(a) 1g (b) 6-VCCTEF-12DV

Figure 11 Pressure Coefficient Contour on the TTBW Geometries at Mach 0.8 and $C_{L_2} = 0.695$

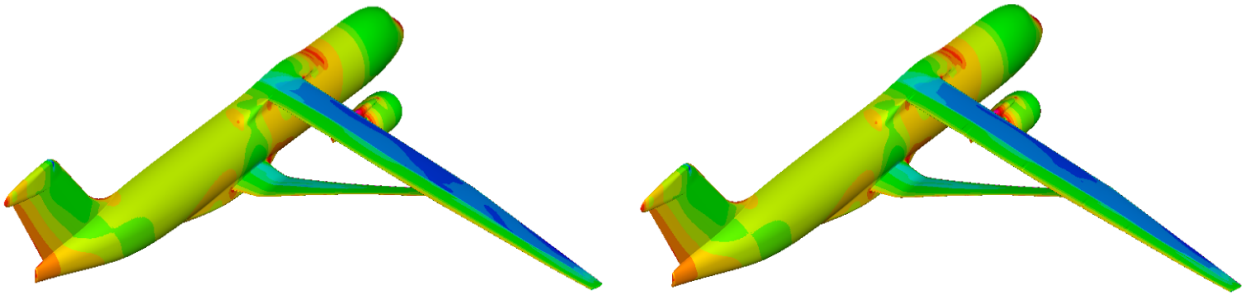

(a) 1g (b) 6-VCCTEF-12DV

Figure 12 Pressure Coefficient Contour on the TTBW Geometries at Mach 0.8 and $C_{L_3} = 0.729$

Table 9 Drag Optimization Results from FUN3D for $C_{L_1} = 0.661$

Model	α(deg.)	C_L	C_D	$\Delta C_{D_{FUN3D}}$(counts)	$\Delta C_{D_{VSPAERO}}$(counts)
1g	1.450	0.661	0.03155	-	-
6-VCCTEF-12DV	2.068	0.661	0.03069	8.6	9.5

Table 10 Drag Optimization Results from FUN3D for $C_{L_2} = 0.695$

Model	α(deg.)	C_L	C_D	$\Delta C_{D_{FUN3D}}$(counts)	$\Delta C_{D_{VSPAERO}}$(counts)
1g	1.710	0.695	0.03261	-	-
6-VCCTEF-12DV	2.109	0.695	0.03185	7.6	9.0

Table 11 Drag Optimization Results from FUN3D for $C_{L_3} = 0.729$

Model	α(deg.)	C_L	C_D	$\Delta C_{D_{FUN3D}}$(counts)	$\Delta C_{D_{VSPAERO}}$(counts)
1g	1.953	0.729	0.03468	-	-
6-VCCTEF-12DV	2.429	0.729	0.03367	10.1	11.2

Conclusions

A drag optimization study for the Mach 0.8 TTBW aircraft with VCCTEF is performed based on the in-house developed tool VSPAERO for rapid aerodynamic analysis. The lift and drag coefficients predicted by the solver agree well with the wind tunnel data for the TTBW aircraft. Three flight conditions corresponding to Mach 0.8 $C_{L_1} = 0.661$, $C_{L_2} = 0.695$, and $C_{L_3} = 0.729$ are used as the focal point for the Mach 0.8 TTBW aircraft VCCTEF optimization study. The optimization results show that the 6-spanwise sections VCCTEF, especially when the deflection angles of the inner and outer segments are directly used as design variables, provides relative better solution for the drag reduction when the actuator weight effects are considered. The high-fidelity CFD solver FUN3D simulation results confirm the drag optimization results obtained by the VSPAERO model.

Acknowledgment

The authors wish to acknowledge NASA Advanced Air Transport Technology project for the funding support of this work. The authors also acknowledge Boeing Research and Technology and in particular Christopher Droney, Neal Harrison, Michael Beyar, Eric Dickey, and Anthony Sclafani, along with the NASA technical POC, Gregory Gatlin, for their research conducted under the NASA BAART contracts NNL10AA05B and NNL16AA04B. The research published in this paper is made possible by the technical data and wind tunnel test data furnished under these BAARTcontracts.

References

[1] Bhatia, M., et. al.. "Structural and Aeroelastic Characteristics of Truss-Braced Wing: A Parametric Study," Journal of Aircraft, Vol 49, No. 1, 2012.

[2] Gundlach, J. F., Tetrault, P. A., Gern, F. H., Nagshineh-Pour, A. H., Ko, A., Schetz, J. A., et. al., "Conceptual Design Studies of a Strut-Braced Wing Transonic Transport," Journal of Aircraft, Vol. 37, No. 6, 2000.

[3] Gur, O., Bhatia, M., Schetz, J.A., Mason, W. H., Kapania, R. K., and Mavris, D. N., "Design Optimization of a Truss-Braced Wing Transonic Transport Aircraft," Journal of Aircraft, Vol. 47, No. 6, 2010.

[4] Harrison, N. A., Beyar, M. D., Dickey, E. D., Hoffman, K., Gatlin, G.M. and Viken, S. A., "Development of an Efficient Mach=0.80 Transonic Truss-Braced Wing Aircraft," AIAA SciTech Conference, AIAA-2020-0011, January 2020.

[5] Nguyen, N., "Elastically Shaped Future Air Vehicle Concept, " NASA Innovation Fund Award 2010 Report, October 2010, Submitted to NASA Innovative Partnerships Program,

[6] Nguyen, N. and Urnes, J., "Aeroelastic Modeling of Elastically Shaped Aircraft Concept via Wing Shaping Control for Drag Reduction," AIAA Atmospheric Flight Mechanics Conference, AIAA-2012-4642, August 2012.

[7] Nguyen, N., Livne, E., Precup, N., Urnes, J., Nelson, C., Ting, E. and Lebofsky, S., "Experimental Investigation of a Flexible Wing with a Variable Camber Continuous Trailing Edge Flap Design, " AIAA 2014-2441, June. 2014

[8] Lebofsky, S., Ting, E., Trinh, K. V., Nguyen, N. T., "Optimization for Load Alleviation of Truss-Braced Wing Aircraft With Variable Camber Continuous Trailing Edge Flap," 33rd AIAA Applied Aerodynamics Confererence, AIAA-2015-2723, June 2015.

[9] Ting, E., Chaparro D., Nguyen, N. T., Fujiwara, G. E., "Optimization of Variable-Camber Continuous Trailing-Edge Flap Configuration for Drag Reduction," Journal of Aircraft, Vol. 55, No. 6, pp. 2217-2239, 2018.

[10] Bartels, R. E., Stanford B. K., Waite, J. M., "Performance Enhancement of the Flexible Transonic Truss-Braced Wing Aircraft Using Variable-Camber Continuous Trailing-Edge Flaps," AIAA 2019-0316, June 17-21, 2019, Dallas, Texas

[11] Xiong, J., Bartels, R. E., and Nguyen, N., "Aerodynamic Optimization of Mach 0.745 Transonic Truss-BracedWing Aircraft with Variable-Camber Continuous Trailing-Edge Flap," AIAA Science and Technology Forum and Exposition, AIAA-2021-0337, Jan. 2021.

[12] Litherland B. and Rieth K., "VSP Aircraft Analysis User Manual,", July. 2014

[13] Fujiwara, G., Chaparro, D., and Nguyen, N., "An Integral Boundary Layer Direct Method Applied to 2D Transonic Small-Disturbance Equations," 34th AIAA Applied Aerodynamics Conference, AIAA-2016-3160, June 2016.

[14] Chaparro, D., Fujiwara, G., Ting, E., and Nguyen, N., "Aerodynamic Modeling of Transonic Aircraft Using Vortex Lattice Coupled with Transonic Small Disturbance for Conceptual Design," 34th AIAA Applied Aerodynamics Conference, AIAA-2016-3012, June 2016.

[15] Chaparro, D., Fujiwara, G. E., Ting, E., and Nguyen, N. T., "Transonic and Viscous Potential Flow Method Applied to Flexible Wing Transport Aircraft," 35th AIAA Applied Aerodynamics Conference, AIAA-2017-4221, June 2017.

[16] Stahara, S. S., "Operational Manual for Two-Dimensional Transonic Code TSFOIL," NASA Contractor Report 3064, December, 1978.

[17] Drela, M., "A User's Guide to MSES 3.05," MIT Department of Aeronautics and Astronautics, July 2007.

[18] Fugate, J., Nguyen, N., and Xiong, J., "Aero-Structural Modeling of the Truss-BracedWing Aircraft Using Potential Method with Correction Methods for Transonic Viscous Flow andWing-Strut Interference Aerodynamics," AIAA Aviation Conference, AIAA-2019-3028, June 2019.

[19] Xiong, J., Nguyen, N., and Fugate, J., "Investigation of Truss-Braced Wing Aircraft Transonic Wing-Strut Interference Effects Using FUN3D," AIAA Aviation Conference, AIAA-2019-3026, June 2019.

[20] Xiong, J., Nguyen, N., and Fugate, J., "Study of Mach 0.8 Transonic Truss-Braced Wing Aircraft Wing-Strut Interference Effects," AIAA SciTech Conference, AIAA-2020-0336, , January 2020.

[21] Theodorsen, T., "General Theory of Aerodynamic Instability and the mechanism of Flutter", NACA Report No. 496, 1949.

[22] Urnes, J., Nguyen, N., Ippolito, C., Totah, J., Trinh, K., and Ting, E., "A Mission Adaptive Variable Camber Flap Control System to Optimize High Lift and Cruise Lift to Drag Ratios of Future N+3 Transport Aircraft," 51st AIAA Aerospace Sciences Meeting, AIAA-2013-0214, January 2013.

[23] Biedron, R. T., et al., "FUN3D Manual 13.2,", NASA TM-2017-219661, Aug. 2017

[24] Lee-Rausch, E. M., Hammond, D. P., Nielsen, E. J., Pirzadeh, S. Z., and Rumsey, C. L., "Application of the FUN3D Unstructured-Grid Navier-Stokes Solver to the 4th AIAA Drag Prediction Workshop cases," AIAA Aviation Conference, AIAA-2010-4511, January 2019.

[25] Roe, P. L., "Approximate Riemann Solvers, Parameter Vectors and Difference Schemes,", Journal of Computational Physics, Vol. 46, No. 2, 1980, pp. 357-378

[26] Venkatakrishnan, V., "Convergence to Steady State Solutions of the Euler Equations on Unstructured Grids with Limiters,", Journal of Computational Physics, Vol. 118, No. 1, 1995, pp. 120-130

[27] Spalart, P. R. and Allmaras, S. R., "A One-Equation Turbulence Model for Aerodynamic Flows," AIAA Science and Technology Forum and Exposition, AIAA-1992-0439, January 1992.